Electric and Magnetic Dipole Strength at Low Energy

K. Sieja
Université de Strasbourg, IPHC, 23 rue du Loess 67037 Strasbourg, France
and CNRS, UMR7178, 67037 Strasbourg, France

(Received 7 March 2017; revised manuscript received 6 May 2017; published 31 July 2017)

A low-energy enhancement of radiative strength functions was deduced from recent experiments in several mass regions of nuclei, which is believed to impact considerably the calculated neutron capture rates. In this Letter we investigate the behavior of the low-energy γ-ray strength of the ^{44}Sc isotope, for the first time taking into account both electric and magnetic dipole contributions obtained coherently in the same theoretical approach. The calculations are performed using the large-scale shell-model framework in a full $1\hbar\omega$ *sd-pf-gds* model space. Our results corroborate previous theoretical findings for the low-energy enhancement of the $M1$ strength but show quite different behavior for the $E1$ strength.

DOI: 10.1103/PhysRevLett.119.052502

Introduction.—Radiative strength functions (RSF) and level densities are fundamental properties of the atomic nucleus that govern the formation and decay of excited nuclei. They are basic inputs for the evaluation of neutron capture cross sections, which are critically important to a breadth of scientific fields. As an example, radiative neutron capture plays a central role in astrophysical models of nucleosynthesis and stellar evolution [1,2]. The knowledge of neutron capture cross sections is necessary to optimize the design of nuclear power reactors and determine the ideal parameters for the burnup of nuclear waste [3]. Direct measurements of neutron capture cross sections are however limited to stable nuclei and those with long half-lives. Thus, most of the applications resort to large sets of theoretical reaction rates that are evaluated based on simple statistical assumptions; e.g., radiative strength functions are described by global parametrizations that can be adjusted to photodissociation data. However, such RSF miss important structure effects at low energy. A decade ago a low-energy enhancement of the RSF was discovered in experiments [4]. With the enhancement established on stable nuclei [5], its nature and extent remain however unknown. In astrophysical settings element formation generally takes place in very neutron-rich regions. The enhanced probability to decay by low-energy γ rays could have dramatic consequences on neutron capture cross sections, altering them by a factor 10 with respect to the predictions of the common theoretical models [6,7].

The nuclear shell model (SM), known as the configuration interaction in other fields, is commonly used to calculate nuclear spectra and transitions at low energy. Recently, a method of obtaining the dipole strength functions from averages of a large number of magnetic dipole ($M1$) transitions within the shell model was proposed [8]. It was shown that in the mass $A \sim 90$ region the $M1$ RSF are enhanced toward low energy, in agreement with experimental observations. It has been suggested that this occurs in nuclei near closed shells where high j proton and neutron orbitals are located near the Fermi surface with magnetic moments adding up coherently. Later calculations in iron nuclei [9] supported the existence of such an enhancement mechanism, called low-energy magnetic radiation (LEMAR) in Ref. [7]. On the other hand, in Ref. [10] the role of electric dipole ($E1$) transitions was studied in the finite-temperature relativistic quasiparticle random phase approximation (QRPA). A temperature dependent broadening of the low $E1$ strength was found in several Mo nuclei. Up until now, calculations of both the $M1$ and $E1$ strength within the same theoretical framework have not been carried out in this context. At present, the shell model is the only microscopic tool that can coherently describe all kinds of electromagnetic transitions between a wealth of excited nuclear states. Nevertheless, the calculations of the $E1$ strength within this framework are scarce due to the necessity of large model spaces, resulting in very complex numerical calculations.

In the present Letter we obtain for the first time the total low-energy $M1$ as well as $E1$ RSF within the large-scale shell model. For simplicity, we focus on one nucleus, ^{44}Sc, for which experimental data are available. The conclusions hold however also for neighboring nuclei studied in the same way (^{43}Sc, ^{44,45}Ti). Our results corroborate previous findings about the important role of the $0\hbar\omega$ $M1$ transitions in low-energy enhancement. On the contrary, we find flatter behavior of the low-energy part of the strength function coming from the magnetic dipole transitions between unnatural parity states. Most importantly, no low-energy upbend is found for the $E1$ strength. Comparison with experiment shows that the current shell model can give a good description of the dipole strength at low energies and explain the structure effects of the RSF, bringing a necessary insight into a domain dominated so far by phenomenological approaches.

Theoretical framework.—We employ the large-scale shell-model framework in the model space comprising

sd-pf-gds orbitals. The interaction used here is based on a realistic set of matrix elements from the charge-dependent Bonn nucleon-nucleon potential (CD-Bonn) [11] softened via the V_{lowk} procedure [12], and adapted to the model space by many-body perturbation techniques, as usually practiced in shell models [13,14]. The Hamiltonian has been further optimized empirically: the initial *pf*-shell matrix elements have been replaced by a recent fit from Ref. [15] and further monopole corrections have been applied to the cross-shell interactions, in order to fix the known positions of single–particle-hole states and of the lowest unnatural parity states. In calculations we have employed the coupled scheme code NATHAN [16]. Full *pf*-shell diagonalizations for the natural parity states have been achieved and the full $1\hbar\omega$ excitations for the opposite parity states have been taken into account. The latter permits exact factorization of the spurious center of mass (c.m.). The shell-model Hamiltonian reads

$$H = \sum_i \epsilon_i c_i^\dagger c_i + \sum_{ijkl} V_{ijkl} c_i^\dagger c_j^\dagger c_l c_k + \beta H_{\mathrm{c.m.}},$$

where the c.m. Hamiltonian with a multiplication coefficient β has been added to push up the c.m. eigenvalues to the energy range not considered here. In the calculations of magnetic transitions effective $M1$ operators have been used; i.e., the spin part of the operator has been quenched with a commonly adopted value of 0.75 [17]. This allows good reproduction of experimentally known magnetic moments in the region.

To obtain the averages of the reduced transition strengths and strength functions we follow the procedure applied previously in Refs. [8,9]. The average $\langle B(M1|E1)\rangle$ values are computed as the sum of all $B(M1|E1)$ values per energy bin of 200 keV divided by the number of transitions within this bin. The RSF are deduced from the relations $f_{M1|E1}(E_\gamma) = 16\pi/9(\hbar c)^3 S_{M1|E1}(E_\gamma)$, where the microscopic strength function $S_{M1|E1}$ (i.e., the strength per energy interval) is obtained as $\langle B(M1|E1)\rangle \rho_i(E_i)$, $\rho_i(E_i)$ being the calculated level density at the energy of the initial state of the excitation energy E_i. We have computed up to 60 states of each parity in the spin range $J = 0$–12. To obtain low-energy averages and strength functions, only states below $E_{\mathrm{exc}} = 10$ MeV were included (the neutron separation energy of ^{44}Sc is 9.7 MeV). This leads to a total of 1078 levels of both parities, 8 6642 $M1$ and 6 5670 $E1$ matrix elements taken into account in further evaluations. For the purpose of illustration, we have also computed the photoabsorption strength function of the ground state using the Lanczos strength function (LSF, see, e.g., [16]) method with 500 iterations.

Results and discussion.—We start the discussion with the average magnetic dipole strength $\langle B(M1)\rangle$: the averages were deduced for both parities separately and are shown in Fig. 1. The natural parity ($0\hbar\omega$) part of $M1$ is clearly

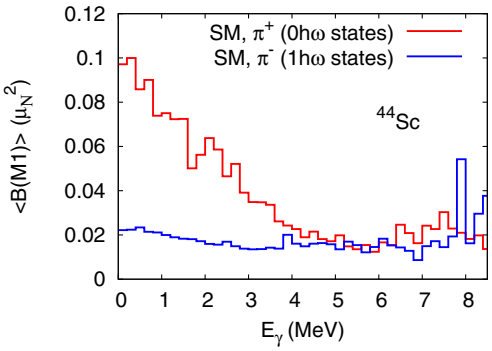

FIG. 1. Averaged $M1$ transition probabilities. The contributions from the natural (π^+) and unnatural (π^-) parity states are distinguished.

enhanced at low energy, in agreement with previous shell-model calculations for Mo and Fe isotopes. The natural parity states contain protons and neutrons in the $f_{7/2}$ orbital, which can be recoupled to generate higher-spin states, leading to many close lying levels connected by $M1$'s involving large $f_{7/2} \rightarrow f_{7/2}$ matrix elements. Such diagonal matrix elements were shown to be responsible for the shape of the lowest part of the $M1$ strength in ^{56,57}Fe (see Fig. 4 in Ref. [9]).

Concerning $1\hbar\omega$ states, they are formed by lifting proton or neutron particles mostly from the $d_{3/2}$ orbit to the $f_{7/2}$ orbit and have wave functions fragmented over many different configurations. This leads to numerous cancellations and involves many smaller, nondiagonal matrix elements in the magnetic transitions. As a result, the unnatural parity magnetic dipole behaves differently: its average magnitude is much lower and the low-energy part much flatter. We have verified that both $M1$ components stay rather constant as a function of the number of states calculated, the cutoff in excitation energy and spin range taken into account (see as well Refs. [18,19]). This is in agreement with the previous shell-model results, which postulated that the low-energy behavior of the magnetic dipole is mostly wave-function dependent [9].

We now focus our attention on electric dipole transitions in the shell model, which have not been investigated in this context so far. First, the theoretical $E1$ strength is shown in Fig. 2. The red curve corresponds to the cumulated $E1$ strength per excitation energy bin obtained from a wealth of low-lying excited states. The blue curve shows the ground state strength function obtained with the LSF method ($1^-, 2^-, 3^- \rightarrow 2^+$ transitions). We note, in passing, that modern microscopic theories like the QRPA, which provide an excellent description of the giant dipole resonances (GDR), face problems in describing the transitions between excited states. In other words, the low-energy strength shown in Fig. 2 cannot be obtained microscopically within the QRPA framework, formally describing the γ absorption

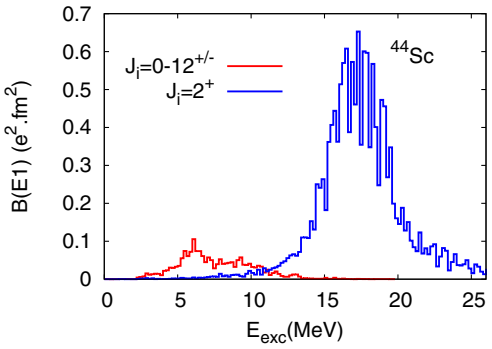

FIG. 2. Cumulated $E1$ transition strength per excitation energy bin. The red curve represents the strength obtained from the wealth of low-lying states in the spin and parity range $J_i = 0{-}12^{+\text{and}-}$. The blue curve corresponds to the strength function for absorption from the 2^+ ground state of ^{44}Sc.

of the ground state (thus corresponding to the LSF of the ground state in the shell model).

We now examine in more detail the behavior of the low-energy strength: in Fig. 3 the averaged $E1$ strength is plotted as a function of transition energy. The averaged strength exhibits a flat trend towards $E_\gamma = 0$, contrary to the natural parity $M1$ shown in Fig. 1. This remains the same when the average is multiplied by the level density, i.e., converted to the strength function shown in Fig. 4. We also display the cuts of the low-energy part of the $E1$ strength as a function of excitation energy. The deviation is largest in the case of excitation energies in the range of 0–5 MeV, where the average strength is a factor of ∼2 higher than for the other ranges at $E_\gamma = 0$. The greater slope of the corresponding f_{E1} is simply due to the lower density of states in this interval, making the higher energy transitions privileged with respect to the lower γ-ray transitions. In the remaining ranges of excitation energies the results stay reasonably close to each other. More importantly, no structure effects comparable to those of the $M1$ strength

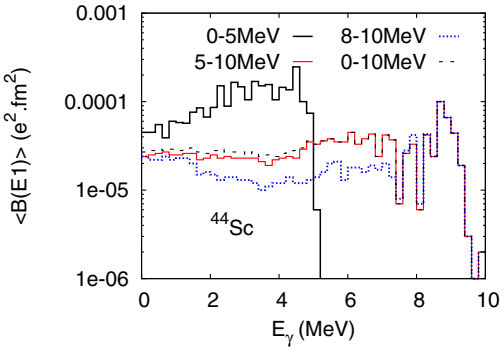

FIG. 3. The average $\langle B(E1)\rangle$ strength as a function of the transition energy (E_γ). In addition to the calculation taking the whole low-energy strength below the neutron separation energy (0–10 MeV), the results obtained with different cuts in excitation energy are shown.

are observed at low energy, independently of the energy cutoff. As in the case of the $M1$ strength, we have verified that this low-energy behavior of the RSF is also robust against the spin range taken into account.

As seen from Fig. 2, the strongest $E1$ matrix elements are those of the GDR with the transition energy of the order of $1\hbar\omega$. The unnatural parity states at excitation energies < 10 MeV are predominantly due to the promotion of the $d_{3/2}$ particle to the $f_{7/2}$ orbit and the natural parity states are dominated by $\pi f^1_{7/2}\nu f^3_{7/2}$ configurations. The typical occupancy of higher pf-shell orbits in those states is of the order of 0.7–1.1 particle for neutrons and does not exceed 0.5 particle for protons. Since the nonvanishing $E1$ matrix elements connect $d_{3/2}$ and $f_{5/2}, p_{3/2}, p_{1/2}$ orbitals, there are no large $E1$ contributions at small transition energies that could produce a low-energy spike in the strength function. On the other hand, the presence of those transitions means that the $E1$ strength does not drop to zero for $E_\gamma = 0$. The decay to all available states below the neutron threshold adds a broad, nonzero component to the $E1$ strength function at low energy. This brings us to the Brink hypothesis [20], which is the basis of the Hauser-Feschbach calculations of neutron capture cross sections and of experimental analyses. This states that the photoabsorption cross section is independent of the excitation energy. Assuming the detailed balance principle the downward and upward strength functions should then be equal. This is obviously not the case here, as can be seen from Fig. 2. The partial breakdown of the Brink hypothesis has previously been discussed in the literature, recently also in the shell-model approach for the $M1$ operator, e.g., in Refs. [9,21].

One should note that the shell model is the only microscopic method that can properly describe both the upward and downward $E1$ strengths. While dealing with the γ decay, a temperature-dependent correction term is traditionally added in the QRPA approaches to describe collisions between quasiparticles [22]. The $E_\gamma \to 0$ limit in this case may exhibit a substantial upbend for $T > 0$. In Ref. [10] the γ emission in the relativistic QRPA was treated as photoabsorption of the state at a finite temperature.

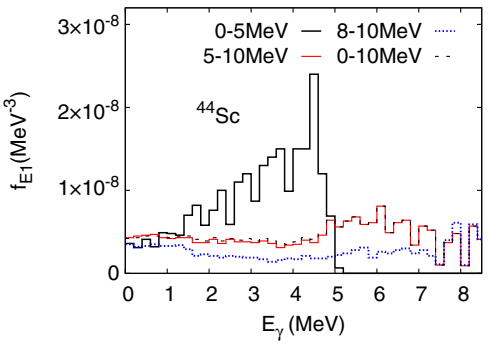

FIG. 4. The same as in Fig. 3 but for the corresponding strength function.

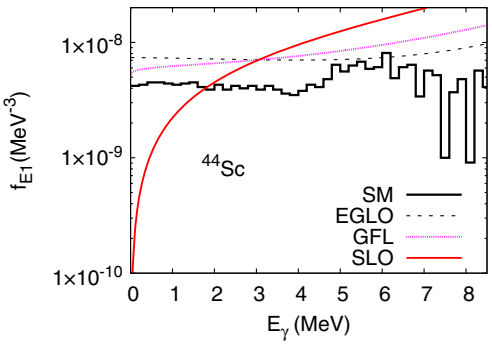

FIG. 5. Comparison of the low-energy f_{E1} obtained from shell-model calculations to the commonly applied global models of RSF. See the text for more details.

A broadening of the strength for $E_\gamma < 1$ MeV has been found, however with the $E1$ strength dropping to zero in the $E_\gamma = 0$ limit. As evidenced by the present results, none of the currently existing treatments of the radiative decay in the QRPA approaches are compatible with the microscopic shell-model findings. This indicates a necessity for a further theoretical understanding of differences between upward and downward strength functions and for a revision of empirical corrections added to describe γ decay using QRPA methods.

Let us now compare the microscopic strength predicted by our calculations to that resulting from other available theoretical calculations. There exist a number of analytic models that describe the γ decay using a global systematics of parameters deduced from the analysis of experimental cross sections. In Fig. 5 we compare the results from the shell model to theoretical predictions from the RIPL-2 library [23]. Shown are the standard Lorentzian (SLO) [24], enhanced generalized Lorentzian (EGLO) [24], and generalized Fermi liquid (GFL) [25,26] models. Among the models, the standard Lorentzian approach appears the least realistic, as the microscopically derived $E1$ strength does not drop to zero in the $E_\gamma = 0$ limit. The GFL and EGLO models reasonably approximate the microscopic shell-model strength, in spite of their (*a priori*) limited predictability for $A < 50$ nuclei.

Finally, we compare the RSF obtained within the shell model to the experimental one, see Fig. 6. Theoretical $M1$ and $E1$ components are distinguished. The $M1$ strength is obtained as an average of f_{M1} for both parities. Taking into account magnetic transitions between the $1\hbar\omega$ states reduces the total f_{M1} without visible influence on its shape at the lowest transition energies. The total SM strength function is obtained as a sum of f_{M1} and f_{E1}. As can be seen, the overall agreement between experiment and theory is good. However, the 0–4 MeV part of the RSF can be accounted for by taking only the magnetic dipole contribution: the $E1$ component adds a small and constant value to the RSF at low energy but does not produce any additional enhancement.

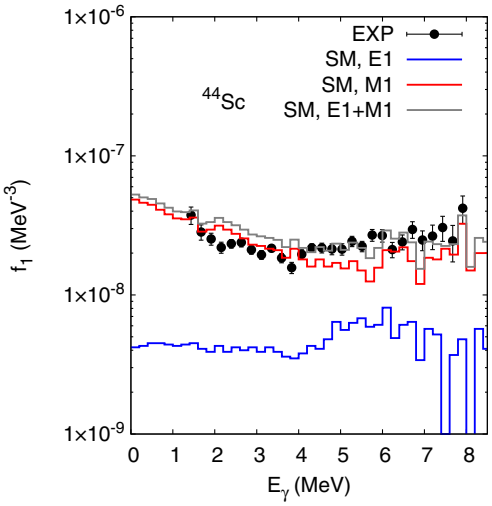

FIG. 6. Comparison of SM results to experimental data for the RSF from Ref. [27]. Theoretical contributions from $M1$ (red) and $E1$ (blue) components are distinguished in addition to the total theoretical RSF (gray line).

Although in the present Letter we have only discussed in detail the results for one nucleus, our conclusions on the behavior of low-energy radiation hold for several nuclei: we computed the dipole strength within the same framework and the results are shown in Fig. 7. No enhancement of the $E1$ radiation at low energy was found either in ^{43}Sc or in ^{44,45}Ti. A visible enhancement of the $0\hbar\omega$ $M1$ is however present in those cases [18,19]. All the calculated f_{E1} exhibit a flat trend toward the small transition energies, with a nonvanishing value at $E_\gamma = 0$. This behavior, independent of the even-even, odd-odd, or even-odd character of the nucleus, is simply connected to the presence of many close-lying excited states of both parities, and thus should hold true for all nuclei with a considerable level density around the neutron threshold. However, it remains to be studied whether the low-energy trend of the $E1$ strength persists far from the stability line, where the neutron intruder states have a decisive role in shaping the low-energy structure of nuclear systems.

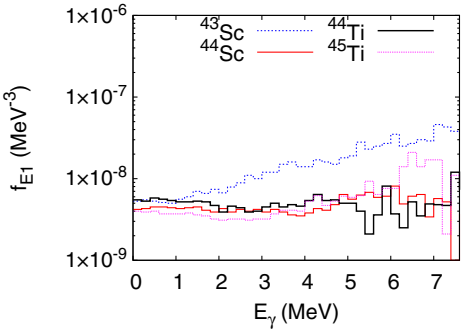

FIG. 7. Low-energy electric dipole strength functions obtained within the present shell-model framework for several mass $A = 43$–45 nuclei.

Conclusions.—We have presented the state-of-the art calculations of the low-energy dipole strength function including the $E1$ and $M1$ contributions obtained within the large-scale shell model in a full $1\hbar\omega$ space. The total radiative strength function obtained from the shell model is shown to be in good agreement with experimental data at low transition energies. For the first time, the $1\hbar\omega$ $M1$ transitions have been studied and shown to impact mostly the magnitude of the total magnetic strength. The electric dipole f_{E1}, also derived for the first time using the shell model, shows a flat behavior towards small transition energies, consistent with EGLO and GFL global models. On the contrary, the demonstrated existence of the non-vanishing tail of the $E1$ RSF for $E_\gamma = 0$ is in variance with the QRPA results commonly employed in applications, indicating a necessity for revision of those approaches. The electric dipole strength does not contribute to the low-energy upbend observed in ^{44}Sc. Therefore, our conclusion is that the $0\hbar\omega$ $M1$ strength is the only part of the dipole strength function that can exhibit enhancement effects comparable with experimental data. The nuclear shell model, presently proven to be a valid tool for the studies of the full low-energy dipole strength, can be further used to examine the evolution of structure effects of RSF further away from the stability line and to quantify the low-energy enhancement and its actual impact on (n, γ) cross sections.

Discussions and exchanges with E. Caurier, G. Martinez-Pinedo, S. Hilaire and S. Goriely are duly appreciated. I thank R. Schwengner for the comments on the manuscript and M. Slupinski for the careful reading and language corrections.

[1] B. Burbidge, G. Burbidge, A. Fowler, and F. Hoyle, Rev. Mod. Phys. **29**, 547 (1957).
[2] M. Arnould, S. Goriely, and K. Takahashi, Phys. Rep. **450**, 97 (2007).
[3] N. Colonna *et al.*, Energy Environ. Sci. **3**, 1910 (2010).
[4] A. Voinov, E. Algin, U. Agvaanluvsan, T. Belgya, R. Chankova, M. Guttormsen, G. E. Mitchell, J. Rekstad, A. Schiller, and S. Siem, Phys. Rev. Lett. **93**, 142504 (2004).
[5] http://www.mn.uio.no/fysikk/.
[6] A. C. Larsen and S. Goriely, Phys. Rev. C **82**, 014318 (2010).
[7] S. Frauendorf *et al.*, Eur. Phys. J. **93**, 04002 (2015).
[8] R. Schwengner, S. Frauendorf, and A. C. Larsen, Phys. Rev. Lett. **111**, 232504 (2013).
[9] B. A. Brown and A. C. Larsen, Phys. Rev. Lett. **113**, 252502 (2014).
[10] E. Litvinova and N. Belov, Phys. Rev. C **88**, 031302 (2013).
[11] R. Machleidt, Phys. Rev. C **63**, 024001 (2001).
[12] S. Bogner, T. Kuo, and A. Schwenk, Phys. Rep. **386**, 1 (2003).
[13] M. Hjorth-Jensen, T. Engeland, A. Holt, and E. Osnes, Phys. Rep. **242**, 37 (1994).
[14] M. Hjorth-Jensen, T. Kuo, and E. Osnes, Phys. Rep. **261**, 125 (1995).
[15] S. M. Lenzi, F. Nowacki, A. Poves, and K. Sieja, Phys. Rev. C **82**, 054301 (2010).
[16] E. Caurier, G. Martinez-Pinedo, F. Nowacki, A. Poves, and A. P. Zuker, Rev. Mod. Phys. **77**, 427 (2005).
[17] G. Martínez-Pinedo, A. P. Zuker, A. Poves, and E. Caurier, Phys. Rev. C **55**, 187 (1997).
[18] K. Sieja, Eur. Phys. J. A (to be published).
[19] K. Sieja, in International Conference on Nuclear Data for Science and Technology (ND2016), Bruges, Belgium, 2016 (2016).
[20] D. Brink, Ph.D. thesis, Oxford University, 1955.
[21] H. P. Loens, K. Langanke, G. Martínez-Pinedo, and K. Sieja, Eur. Phys. J. Spec. Top. **48**, 34 (2012).
[22] S. Goriely, E. Khan, and M. Samyn, Nucl. Phys. **A739**, 331 (2004).
[23] https://www-nds.iaea.org/RIPL-2/.
[24] Handbook for Calculations of Nuclear Reaction Data, RIPL.IAEA-TECDOC-1034, August 1998, http://www-nds.iaea.or.at /ripl/.
[25] F. Mughabghab and C. L. Dunford, Phys. Lett. B **487**, 155 (2000).
[26] V. A. Plujko, Nucl. Phys. **A649**, 209 (1999).
[27] A. C. Larsen *et al.*, Phys. Rev. C **76**, 044303 (2007).